A Horizontal-Winding Multipermeability LTCC Inductor for a Low-profile Hybrid DC/DC Converter

Laili Wang, *Member, IEEE*, Zhiyuan Hu, *Student Member, IEEE*, Yan-Fei Liu, *Fellow, IEEE*, Yunqing Pei, *Member, IEEE*, Xu Yang, *Member, IEEE*, and Zhaoan Wang, *Senior Member, IEEE*

***Abstract*—Distributed air-gap inductors have the advantage of reducing winding loss in high switching frequency dc/dc converters. However, they also have the disadvantage of uneven distribution of flux density, which inevitably leads to uncompleted utilization of magnetic material. This paper proposes a horizontal-winding multipermeability low-temperature cofired ceramic (LTCC) inductor to increase inductance and improve efficiency without the necessity of increasing inductor volume. For the purpose of simplicity, a two-permeability LTCC inductor is taken as an example for analysis and comparison. Design of such an inductor is demonstrated with the aid of 2-D finite elementary analysis simulation. A two-permeability LTCC inductor together with a single-permeability LTCC inductor is fabricated for measuring and testing. The measured results show the two-permeability inductor has higher inductance than the single-permeability inductor. Both inductors are tested in a 5-V input, 3.3-V output dc/dc converter to test their performances. The testing results show the two-permeability LTCC inductor could further improve the efficiency of high-frequency dc/dc converters compared with the single-permeability LTCC inductor.**

***Index Terms*—Efficiency improvement, hybrid integration, low-temperature cofired ceramic (LTCC), planar inductor.**

I. Introduction

ON BOARD converters or power modules are often used to provide power for application-specified integrated circuits (ASICs) and CPUs which are commonly used in portable electronic devices. With the purpose of saving energy and enhancing portability, today's industry requires high light-load efficiency and low profile on board dc/dc converters and power modules. Due to the fact that the portable electronics (such as cell phone, laptop) often operate under stand-by mode, high light-load efficiency is very important for energy saving and increasing battery life [1]. With the technology development of power semiconductors, the package of power MOSFETs has been dramatically reduced; thus, the volume of the converters dominated by active devices shrinks significantly [2]. However, in the past decades, the technology for the passive components has not been improved much. As a result, the passive components have become the major obstacle for increasing power density and lowering the profile. In conventional high-frequency dc/dc converters, the filter inductors are usually constructed with high-permeability commercial magnetic cores and copper wires. These inductors are bulky and reduce power density of power converters indirectly since it is much higher than other components in the converters. In addition, leakage flux from air-gap causes high winding loss and reduces efficiency of converters. In order to further increase the power density, reduce winding loss and production cost, various planar distributed air-gap inductors have been developed [3]–[26]. They could be classified into three categories by the fabricating technology: PCB technology, silicon technology and low-temperature cofired ceramic (LTCC) technology. Inductors based on PCB technology include low-permeability chip inductors and the embedded inductors fabricated with new PCB compatible magnetic materials. Chip inductors are widely used in today's converters for their low cost and easy fabrication [27], [28]. They are laminated with high-flux density iron powder together with copper windings in spiral or solenoid form. For the adoption of low-permeability iron powder, there is no need to use an air-gap in the magnetic core, so the inductors are automatically self-shielding, and have low winding loss for their distributed air-gaps. The major disadvantage of the chip inductors is that they are not compatible for system hybrid integration. For this reason, some materials which could be compatible with PCB manufacture process have been devised, MagLam and flexible polymer compound (FPC) [29] are two of them. A prototype of embedded inductor made with MagLam is shown in [8]. Unfortunately, it has high core loss according to the test result. The FPC also shows the same disadvantage. Inductors based on silicon technology are made by depositing ferrite compound and copper paste on silicon. These inductors have the advantages of high-power density, low cost and high integration level and could be easily integrated into power supply-in-package (PwrSiP) and power supply-on-chip (PwrSoc) converters [3], [4], [22], [24], [26]. The problem for this kind of inductor is its winding resistance is very high, thus the power capacity is very limited. Compared with PCB and silicon technologies, the LTCC technology is more suited for system hybrid integration since it could cofire ceramic tapes, capacitor tapes, and ferrite tapes together to make a passive substrate, which exhibits the same temperature expansion coefficient (TEC) with silicon [11]. Fig. 1 shows an integrated dc/dc

Manuscript received June 10, 2012; revised October 25, 2012 and January 1, 2013; accepted January 2, 2013. Date of current version February 15, 2013. Recommended for publication by Associate Editor D. Perreault.

L. Wang, Z. Hu, and Y.-F. Liu are with the Department of Electrical and Computer Engineering, Queen's University, Kingston, ON K7L 3N6 Canada (e-mail: l.l.wang@queensu.ca; zhiyuan.hu@queensu.ca; yanfei.liu@queensu.ca).

Y. Pei, X. Yang, and Z. Wang are with the Department of Electrical Engineering, Power Electronics and Renewable Energy Center, Xi'an Jiaotong University, Xi'an, Shaanxi 710049, China (e-mail: peiyq@mail.xjtu.edu.cn; yangxu@mail.xjtu.edu.cn; zawang@mail.xjtu.edu.cn).

Color versions of one or more of the figures in this paper are available online at http://ieeexplore.ieee.org.

Digital Object Identifier 10.1109/TPEL.2013.2238640

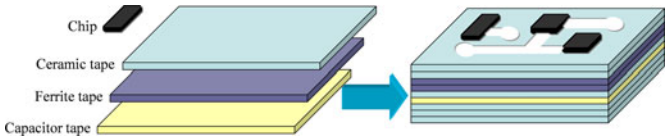

Fig. 1. Structure of an integrated dc/dc converter based on LTCC technology.

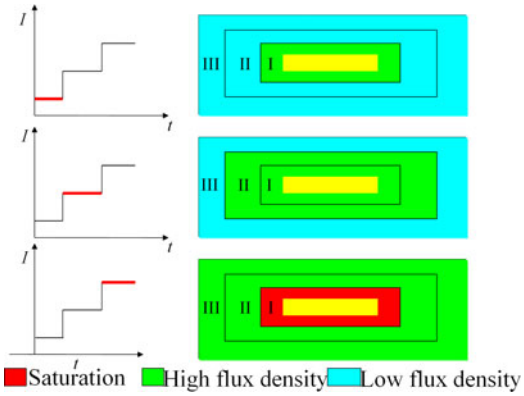

Fig. 2. Flux density distribution of the magnetic core.

converter based on LTCC technology. Recently, passive integration based on LTCC technology has become a hot research topic. Reference [14] presented a design of multiturn LTCC inductors. Reference [15] improved the fabricating process to reduce direct current resistance (DCR) and discussed the effect of cross-sectional shape of conductor on winding loss. [19] proposed the concept of 3-D hybrid integration based on LTCC technology. According to the theory of magnetic circuit, as the perimeter of the conductor decreases, the magnetic resistance increases, and the inductance value at light load increases, too. For this reason, [16] proposes to increase light-load inductance by reducing the width of the conductor. This method could help improve the light-load efficiency, but it also has some negative effects. First, by reducing the width, the conductor resistance will be increased. The increased conductor resistance may not significantly influence the light-load efficiency, but it seriously reduces the full load efficiency. Second, the decrease of the conductor width also makes the magnetic flux density in the magnetic core distribute more unevenly. The magnetic material far away from the conductor is not fully utilized even when the magnetic material close to the conductor has become saturated. Fig. 2 illustrates such a situation in the planar magnetic core. The cross-section of the magnetic core is roughly divided into three regions. At light load, the magnetic material in Region I has high-flux density while that of Regions II and III has lower flux density. At intermediate load, the magnetic material of Region I and Region II has the higher flux density, but the flux density in Region III is still very low. At full load, Region II and Region III has high-flux density, but the magnetic material of Region I has become saturated. In summary, the magnetic core could not be utilized effectively for the whole load range. To fully utilize the magnetic material and increase light-load inductance, this paper proposes a horizontal-winding multipermeability planar inductor structure based on LTCC technology. By using the multipermeability inductor, the light-load inductance could be increased without the necessity of reducing conductor width.

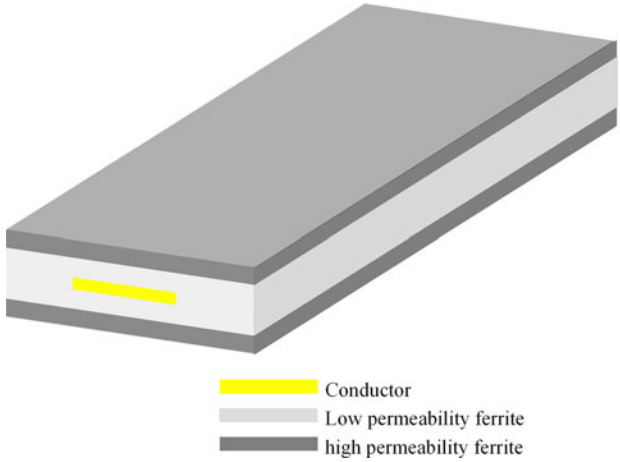

Fig. 3. One-turn two-permeability inductor based on LTCC technology.

Section II of this paper compares four different structures of single-permeability inductors and two-permeability inductors based on finite element analysis (FEA) simulation. Based on the results, the R/L, core loss and winding loss of the inductors are further explored; Section III discusses the inductor fabrication process and shows the test results of the prototypes; finally, conclusion is given in Section IV.

II. Principle and Performances of Horizontal Winding Multipermeability Inductor

A. Planar LTCC Inductor Structures

LTCC is a high-density layer-by-layer lamination, cofiring package technology. A general multipermeability inductor based on LTCC technology can be made by arranging ferrite tapes from an inner layer to the outer layer with permeability gradually increasing. For the purpose of simplicity, this paper only focuses on a two-permeability LTCC inductor shown in Fig. 3. It simplifies to substituting the outer layer of a single-permeability inductor with higher permeability ferrites. By doing this, the flux density distribution in the magnetic core becomes more uniform and the inductance value could be increased. Therefore, the efficiency of a high-frequency dc/dc converter could be improved.

This section analyzes the inductance, resistance, of single-permeability LTCC inductors and two-permeability LTCC inductors of different structural configurations to show the benefit of the proposed method using computer simulation. For the fairness of comparison, both the single-permeability inductors and two-permeability inductors are assumed to have the same thickness. Under this assumption, four structures of one-turn inductors are analyzed in this paper. Two kinds of ferrite tapes are chosen to design the inductor. One is 40010 [30] whose permeability is roughly 50, while the other one is 40011 [31] whose permeability is roughly 200 (the permeability is highly dependent on cofiring temperature profile). Both of them are from ESL ElectroScience Company. In the following text, the

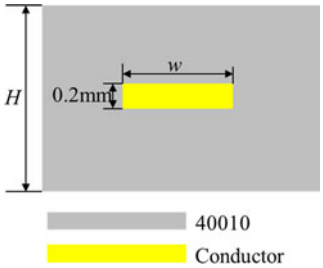

Fig. 4. Cross-sectional view of single-permeability inductor.

two-permeability inductor is designed with 40010 and 40011 while the single-permeability inductor for comparison is made with 40010.

For single-permeability inductors, two cases of structures are considered.

Case I: Varying the conductor width while keeping the conductor thickness constant;

Case II: Varying the conductor width while keeping the cross-sectional area of the conductor constant.

Correspondingly, for two-permeability inductors, there are also two cases.

Case III: Varying the thickness of the different permeability magnetic materials while keeping the conductor thickness constant.

Case IV: Varying the thickness of the different permeability magnetic materials while keeping the cross-sectional area of the conductor constant.

Since the LTCC tapes shrink during the cofiring process (different materials have different shrinkage coefficients, for the ferrite tapes in this paper, the shrinkage coefficient is 17%), the substrate laminated with LTCC tapes may crack if it is too thick, or the conductor buried in it is too wide or thick. LTCC substrate is generally designed no thicker than 3 mm (the thickness is highly related to the fabrication condition and equipment); the conductor is not wider than 5 mm, and not thicker than 1 mm. In the four cases analyzed in this paper, the thickness of the planar inductors is set to be 2 mm. In Cases I and III, the thickness of the conductor is 0.2 mm. In Cases II and IV, the cross-sectional area of the conductor is 0.8 mm^2.

Case I: *Single permeability, 0.2-mm-thick conductor, varying the conductor width*

Case I is also the method employed in [16] to improve the light-load efficiency. Fig. 4 shows the structure of the inductor. The perimeter of the conductor can be expressed by (1)

$$l = 2h + 2w \tag{1}$$

where w is the width of the conductor and h is the height of the conductor. Decreasing w while keeping h constant will decrease l correspondingly. Fig. 5 shows the conductor perimeter versus conductor width. It can be observed that the conductor perimeter decreases linearly with the reduction of the conductor width. As the conductor perimeter reduces, the length of magnetic circuit is also reduced, thus the light-load inductance could be increased; however, the full load inductance may decrease when the conductor width is too small. A magneto static simulation is set up

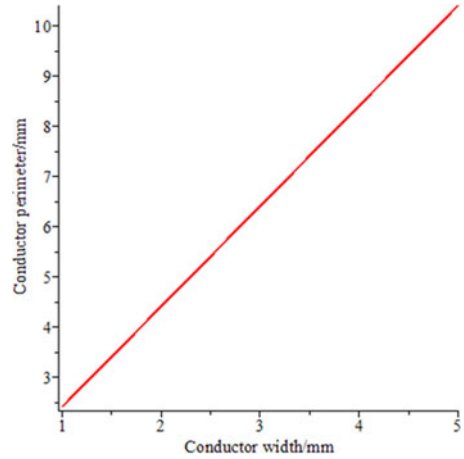

Fig. 5. Perimeter versus conductor width.

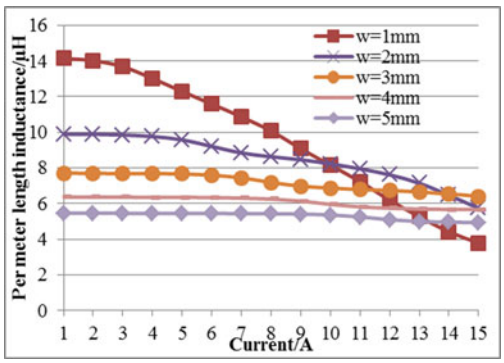

Fig. 6. Per meter length inductance as a function of output current with conductor width as a parameter ($H = 2$ mm).

to calculate the inductance versus conductor width and output current. The magnetic core is made of 40010 whose permeability is 50. The length of the magnetic core is 1 m. Two parameters are swept in the simulation; they are the output current, and the conductor width. Five inductance value curves versus output current are obtained. Fig. 6 shows the results. As the width of the conductor reduces, magnetic reluctance becomes lower and lower, and the light-load inductance gradually increases. The inductor has the highest light-load inductance when $w = 1$ mm, but it quickly reduces with the increase of the output current, and at full load, its inductance becomes the smallest, which may result in higher voltage ripple and stop the electronic devices from working if the inductor is used in a dc/dc converter. Another disadvantage of smaller conductor width configuration is its high DCR which is expressed as

$$R_{\mathrm{DCR}} = \frac{\rho l}{S} \tag{2}$$

where ρ is the resistivity of the silver (1.64e-8 Ω/m), l is the length of the conductor (1 m), and S is the cross-sectional area of the conductor ($w \times 0.2$ mm^2).

Table I lists the per meter length DCR versus conductor width. When the conductor width is higher than 3 mm, the inductance does not change too much, and thus cannot be used to improve light-load efficiency.

TABLE I
PER UNIT LENGTH OF THE DCR

Conductor width/m	1	2	3	4	5
DCR/mΩ	82	41	28	20	16

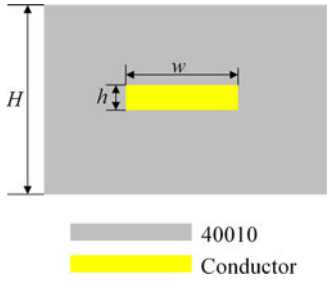

Fig. 7. Cross-sectional view of a single-permeability inductor.

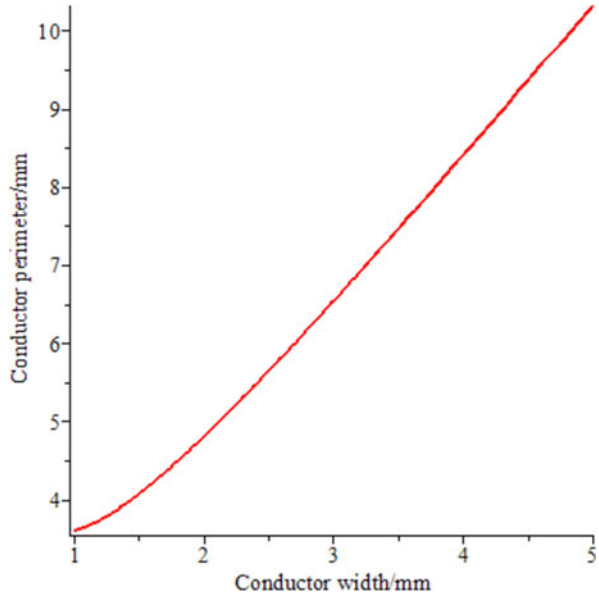

Fig. 8. Conductor perimeter versus conductor width.

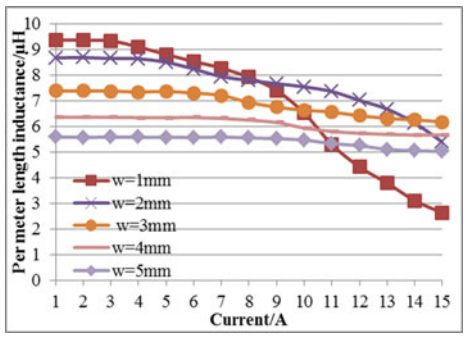

Fig. 9. Per meter length inductance as a function of output current with conductor width as a function.

Case II: Single permeability, 0.8-mm^2-conductor cross-sectional area, varying conductor width

Since Case I only reduces conductor width without changing the conductor thickness, it is inevitable to increase the resistance of the inductor. For this reason, Case II reduces the conductor width while keeping the cross-sectional area of the conductor constant so that the resistance of the conductor does not change. Fig. 7 shows the structure of the inductor.

The cross-sectional area can be expressed by

$$S = wh. \tag{3}$$

The width of the conductor can be derived from (3); it can be expressed as

$$h = \frac{S}{w}. \tag{4}$$

Substituting (4) into (1) yields

$$l = 2w + \frac{2S}{w}. \tag{5}$$

Keeping the cross-sectional area S constant, when w increases from 1 to 5 mm, l will decrease as Fig. 8 shows, and the inductance will also decrease correspondingly. A similar simulation as in Case I is also set up to calculate the inductance values. The magnetic core is still made of 40010, and the length of the magnetic core is still 1 m. Inductors with different combination of conductor width and conductor height under condition that they have the same cross-sectional area are simulated. Fig. 9 shows the per unit length inductances as a function of output current with conductor width as a parameter. Compared with Case I, the corresponding light-load inductance for narrow conductor widths ($w = 1$ mm, $w = 2$ mm) are reduced. This is because in Case II the conductor thickness increases with the decrease of the conductor width to maintain the same cross-sectional area of the conductor. Increasing the conductor thickness will reduce the ferrite thickness above and below the conductor, leading to smaller inductance values than those in Case I. Especially for $w = 1$ mm, where the inductance was reduced the most. For wider conductor configurations, the inductance is nearly the same as those in Case I because the effect of thickness variation to inductance value becomes much less significant. Different from Case I, the per meter length DCR in Case II is constant, it is 0.02 Ω.

Case III: Two-permeability, 0.2-mm-conductor thickness, varying conductor width

The simulation and analysis in Cases I and II indicate that compromise between light-load inductance and conductor width has to be made during the design of single-permeability planar inductors. When the conductor width is large, the inductance does not notably change through the whole load range. Thus, light-load inductance is too low to be used for improving efficiency. To increase the inductance, conductor width should be reduced. When the conductor width becomes smaller, Case I has higher inductance and could be used to improve light-load efficiency, but at the price of increasing DCR, which will reduce the full load efficiency. Case II seems more reasonable because it increases inductance without changing the cross-sectional area of the conductor, although the increase of light-load efficiency is not as high as that in Case I. But when the conductor width is

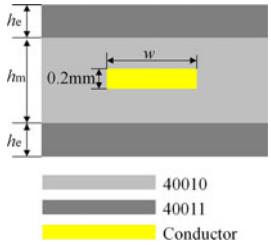

Fig. 10. Cross-sectional view of a two-permeability inductor with constant conductor thickness.

decreased to low level ($w = 1$ mm, $w = 2$ mm), the magnetic core is subject to saturation, leading to low inductance at full load. So intermediate values (such as $w = 3$ mm, $w = 4$ mm) should be chosen. To make the flux density in magnetic core more evenly distributed and to increase inductance, as shown in Fig. 10, low-permeability ferrite tapes of outer layer 40010 are substituted by high-permeability ferrite tapes 40011 on the condition that the thickness of the inductor is not increased ($H = h_m + 2h_e$). For equivalent comparison, two cases of two-permeability inductors are considered. A new magneto static simulation is set up to calculate the inductance versus conductor width and output current. In this case, the magnetic core is made of 40010 whose permeability is 50, and 40011 whose permeability is 200. The length of the magnetic core is 1 m. Three parameters are swept in the simulation. They are the output current, the conductor width, and the thickness of the high-permeability magnetic material 40011. Fig. 11 illustrates per meter length inductance as a function of output current with conductor width as a parameter. Compared with inductors of the same conductor width in Case I, the light-load inductance values are increased by about 30%. But they also have the same disadvantage since they have the same conductor cross-sections with those in Case I, take the inductor with $w = 2$ mm as an example; in Case I, the per meter length inductance at 1 A output current is 10 μH. In Case III, the value depends on the thickness configurations of the different permeability. The lowest value is 13 μH under the condition that $h_m = 1.6$ mm, h_e is 0.2 mm while the highest value is 17 μH under the condition that $h_m = 1.0$ mm and $h_e = 0.5$ mm.

Case IV: Two-permeability, 0.8-mm^2-conductor cross-sectional area, varying conductor width

Similar to Case II, two-permeability inductors with constant cross-sectional area conductor are also simulated for comparison. In this case, the magnetic core is still composed of 40010 whose permeability is 50, and 40011 whose permeability is 200. Three parameters are swept in the simulation. They are the output current, the conductor width (under the condition that the cross-sectional area is constant), and the thickness of the high-permeability magnetic material 40011 (under the condition that the total thickness is constant). Fig. 12 shows the structure. Fig. 13 shows per meter length inductance as a function of output current with conductor width as a parameter. The inductors have higher light-load inductance than those of Case II. With the increase of the thickness of the high-permeability ferrite tapes, the light load inductance is higher, but the full load inductance also drops more. The benefit of two-permeability structure is

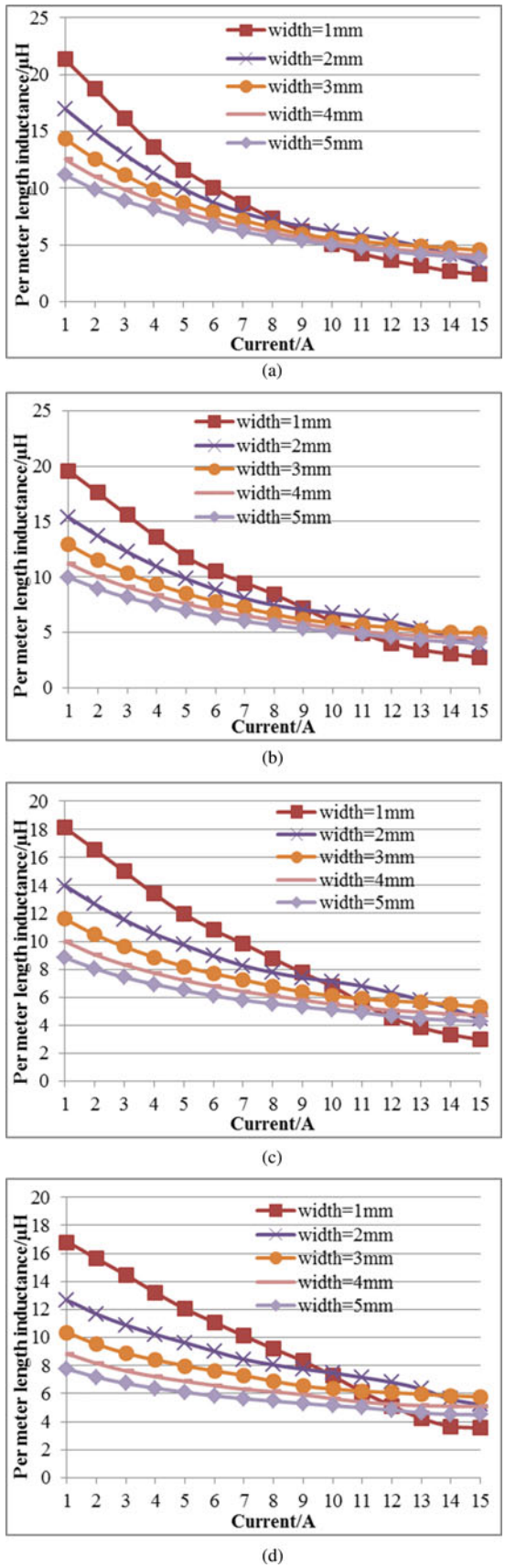

Fig. 11. Per meter length inductance versus output current for a two-permeability inductor. (a) $h_m = 1.0$ mm. (b) $h_m = 1.2$ mm. (c) $h_m = 1.4$ mm. (d) $h_m = 1.6$ mm.

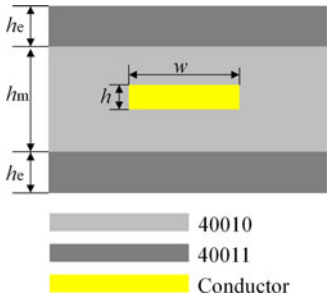

Fig. 12. Cross-sectional view of a two-permeability inductor with constant conductor thickness.

significant. Compared with Case III, the inductors in Case IV have a little bit lower inductance when the conductor width is smaller than 4 mm. The inductance is nearly the same as the conductor width is higher than 4 mm.

B. Comparison of L/R of Four Cases for Selected Conductor Widths

Inductor winding resistance is also a very important parameter to be considered during the designing process of a filter inductor since it determines a fairly large component of the inductor loss. It can be observed from the aforementioned analysis that there is a compromise between the conductor width and thickness. For Cases II and IV, the conductor resistance is smaller, but the inductances are not as high as those in Cases I and III when the conductor width is smaller than 4 mm. To make fair comparison, inductance value should also be considered. In this subsection, L/R is selected as criteria for the comparison of the four cases. According to the inductance curves illustrated earlier, it is reasonable to make the comparison with a selected conductor width of 2, 3, and 4 mm. Fig. 14 shows the L/R curves for these three configurations of conductor widths.

Several trends could be observed from Fig. 14 as following:

1) for single-permeability inductors, Case II (0.8-mm^2 conductor cross-sectional area) has higher L/R than Case I (0.2-mm thick conductor);
2) for two-permeability inductors, Case IV (0.8-mm^2 conductor cross-sectional area) has higher L/R than Case III (0.2-mm conductor thickness);
3) case II has the highest high load inductance; however, its light-load inductance is not high enough, which is not good for improving light-load efficiency;
4) for two-permeability inductors, the inductances exhibit high nonlinearity. The varying ranges of the nonlinear inductances depend on the conductor widths. For the same core structure, the smaller the conductor width, the higher the light-load inductance, and for the same reason, the lower the high-load inductance.

It can be seen that there is a tradeoff for the design of a two-permeability inductor. Higher light-load inductance is necessary for improving light-load efficiency; however, the inductance at high load should also be taken into consideration. For further analysis and comparison, loss of the inductor will be discussed further.

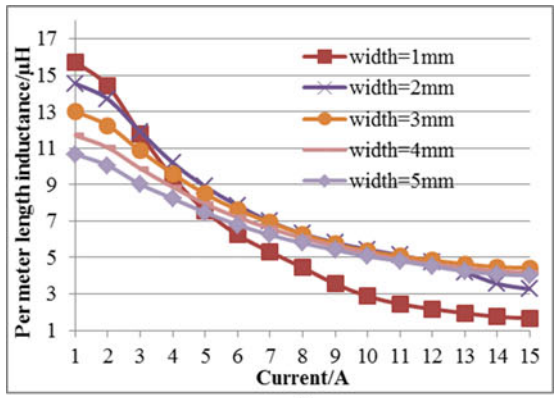

Fig. 13. Per meter length inductance versus output current for a two-permeability inductor. (a) $h_m = 1.0$ mm. (b) $h_m = 1.2$ mm. (c) $h_m = 1.4$ mm. (d) $h_m = 1.6$ mm.

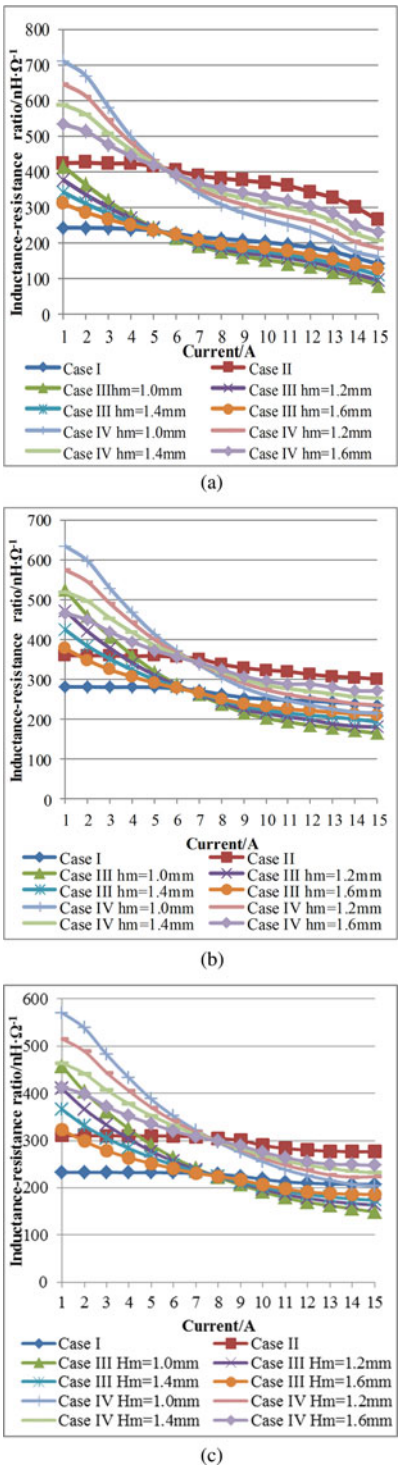

Fig. 14. L/R of the four structures. (a) $w = 2$ mm. (b) $w = 3$ mm. (c) $w = 4$ mm.

C. Core Loss and Winding Analysis of the Inductors

The aforementioned analysis has shown that Case IV (2-mm-total thickness, 0.8-mm^2 conductor cross-sectional area, 1-m length) has higher L/R value; therefore, it is chosen for further analysis. Besides inductance and L/R, the loss is also an important index for evaluating the performances of inductors. Total loss of an inductor is composed of core loss and winding loss. The Stementz equation expressed in (6) is commonly used to calculate the core loss under sinusoidal current excitations [32]

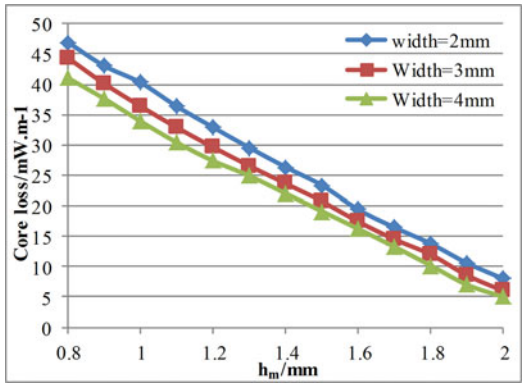

Fig. 15. Core loss as a function of h_m with conductor width as a parameter.

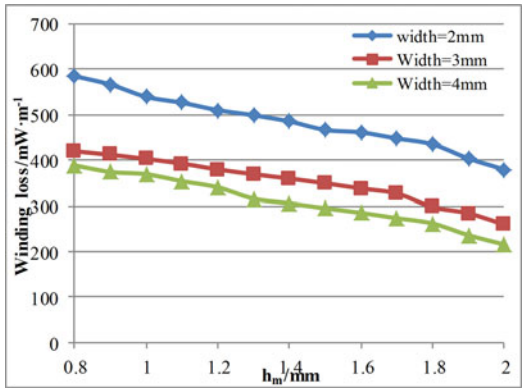

Fig. 16. Winding ac loss as a function of h_m with conductor width as a parameter.

$$P_v = k f^{\alpha} B_m^{\beta}. \tag{6}$$

In this part, a transient type 2-D FEA simulation with conductor width w and thickness of the middle layer magnetic core h_m as sweep parameters is set up to calculate the core losses. In the simulation software itself, the core loss is obtained by employing the Stementz equation (substituting the stimulated ac flux density into the equation). The Stementz parameters for 40010 are $k = 3.99$, $\alpha = 1.113$, and $\beta = 2.673$, while the parameters for 40011 are $k = 1.91 \times 10^{-5}$, $\alpha = 1.905$, and $\beta = 2.271$ [33]. In this simulation, a 3 A, 1-MHz sinusoidal current waveform excitation is applied to the inductor to inspire ac flux density. The simulation results are shown in Fig. 15. With the increase of h_m (the decrease of h_e), the core losses have a decreasing trend. For the same thickness of h_m, the core losses increase with the decrease of conductor width which is also the same with the variation trend of light-load inductance.

Compared with air-gap inductors, the distributed air-gap inductors have much lower winding ac resistance for its reduction of fringing effect. The two-permeability inductors could increase light-load inductance by increasing the flux density of the outer layer in the magnetic cores. However, they may also increase the ac winding loss for the same reason. Fig. 16 shows

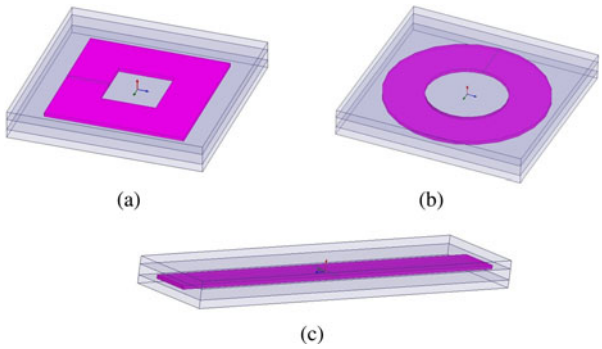

Fig. 17. Models of the three inductors with different winding forms.

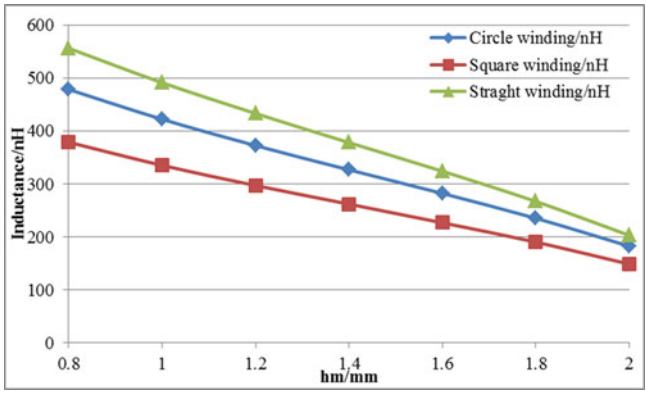

Fig. 18. Inductance versus thickness of the middle layer.

the winding loss versus h_m with conductor width as a parameter. It can be observed that the winding losses also decrease as the h_m increases for all three conductor-width cases. The lowest winding loss occurs when $h_m = 2$ mm, which represents the case of single-permeability inductor.

D. Effect of the Winding Geometry on Inductor Values

For the practical design, the inductor is often designed in spiral shape instead of straight line to save the space. In this part, three inductors of different winding forms (square, circle, and straight) are simulated to evaluate the effect of the winding geometry on inductor performance. Fig. 17 shows the simulated models of the three inductors. They all have the same volume (392 mm^3), the same magnetic core thickness (2 mm), the same winding length (28 mm, medium line), and the same conductor width (3 mm). Inductances versus middle layer thickness (under the condition that total thickness of the magnetic core is 2 mm and the current excitation is 1 A) are simulated. The results are shown in Fig. 18. It can be observed that the inductance values gradually decrease with the thickness increase of the middle layer no matter which winding form is adopted, which implies that the benefit of the multipermeability structure is available for all the three winding forms. However, the winding geometries do have an effect on the inductor values. The straight winding inductor has the highest inductance, while the square winding inductor has the lowest inductance. Between them is the circle winding inductor.

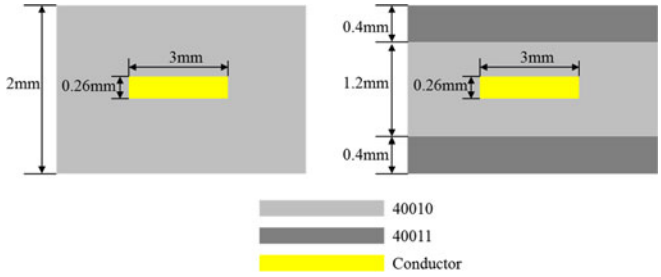

Fig. 19. Dimensions of the single-permeability and two-permeability inductors.

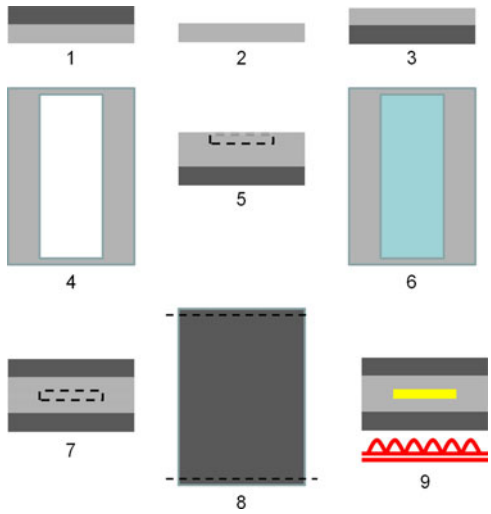

Fig. 20. Fabricating process of the two-permeability inductor.

III. Prototype Fabrication and Experiment

In this section, a two-permeability inductor will be fabricated to evaluate its benefit for increasing inductance value and improve system efficiency. According to the analysis executed previously, the conductor width is selected to be 3 mm and the h_m is selected to be 1.2 mm. And for the purpose of comparison, a single-permeability inductor of the same profile and conductor width is also fabricated. Cross-sectional views of the two inductors are shown in Fig. 19. The single-permeability inductor is made with 40010. The internal layer for the two-permeability inductor is 40010, while the outer layer is 40011. The fabrication process of a single-permeability inductor has been presented in [7]. Here, the fabrication process of the two-permeability inductor shown in Fig. 20 is described as follows:

1) first, three main layers are laminated separately. The first one is laminated with eight layers of 40011 on the top and nine layers of 40010 on the bottom;
2) the second one is laminated with five layers of 40010;
3) the third layer is laminated with nine layers of 40010 on the top and eight layers of 40011 on the bottom;
4) a slot of 35-mm length multiplied by 3-mm width is cut in center of the second layer;
5) the second layer is laminated on the third layer;

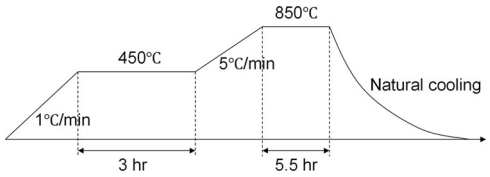

Fig. 21. Temperature profile for cofiring.

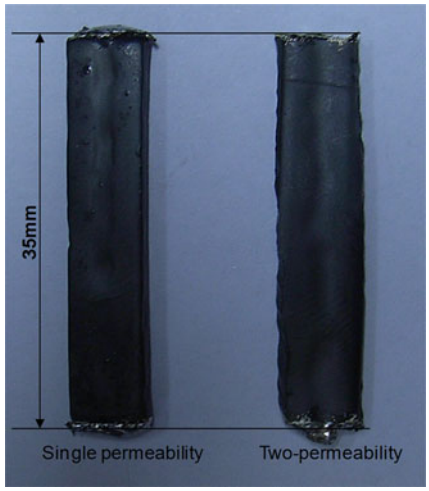

Fig. 22. Prototypes of single-permeability and two-permeability inductors.

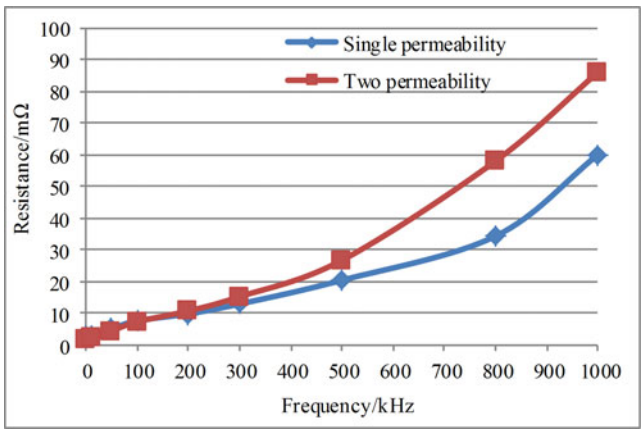

Fig. 23. AC resistances of the single-permeability and two-permeability inductor.

6) the slot is filled with silver paste and then dried in an oven. After the drying process, the silver paste may shrink, repeating the operation so that the silver fully fills the slot;
7) put the first layer on the top of the second layer and laminate them together. Put the whole laminated inductor into a furnace for cofiring according to the temperature profile shown in Fig. 21.

Fig. 22 shows the picture of the inductors. The ac resistances of the two inductors at up to 1 MHz frequency are measured with LCR meter Fluke PM6306 for comparison. The results are shown in Fig. 23. Caused by the high-flux density distribution in the magnetic core, the two-permeability inductor has higher ac resistance than the single-permeability inductor does. At 1 MHz, the two-permeability inductor has ac resistance 86 mΩ, while the single permeability only has 60 mΩ. To obtain the inductance versus output current curve, the two inductors are used in a buck converter to test its current ripple amplitude during the ON time to calculate inductances at different output current. Fig. 24 shows the test results. It can be observed that the two-permeability inductor has much higher inductance at light load.

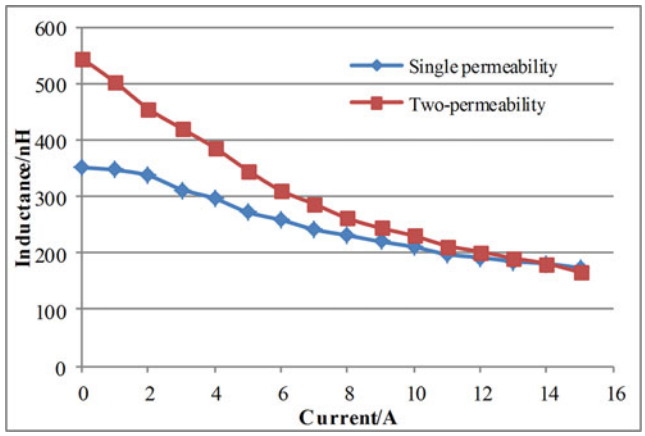

Fig. 24. Inductance versus output current.

TABLE II
PARAMETERS OF SWITCHES SELECTED IN THE CONVERTER

Part number	$R_{ds(on)}$ (mΩ)	Q_{sw} (nC)	Q_g (nC)	Q_{oss} (nC)	Q_{rr} (nC)
BSC080N03MS (Q1)	9.6	5.8	10	17	10
BSC014N03MS (Q2)	1.75	35	84	70	30

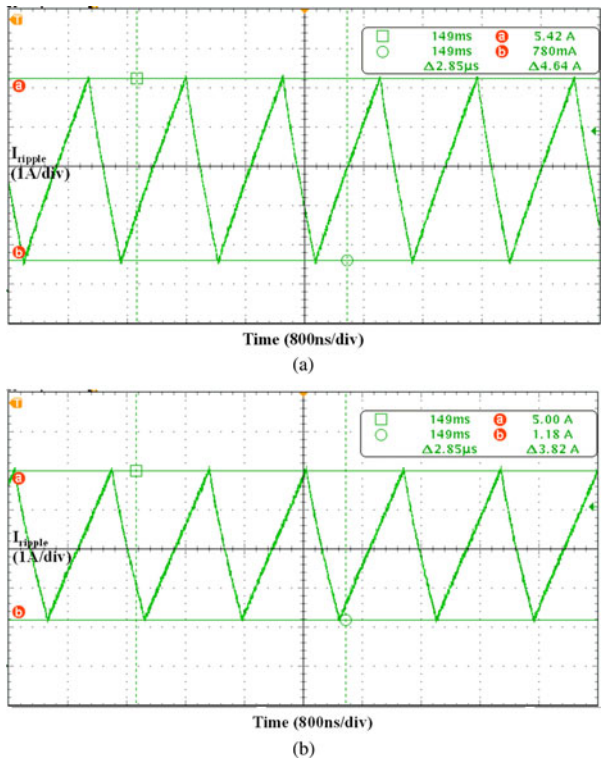

Fig. 25. Current ripple of the inductors at 3 A output current. (a) Single-permeability inductor. (b) Two-permeability inductor.

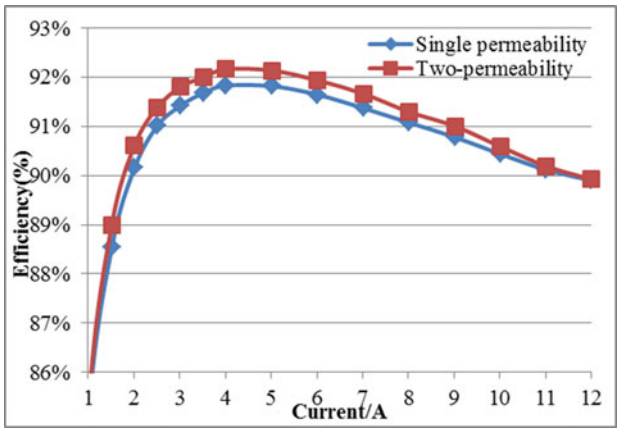

Fig. 26. Efficiencies of the converter with the two inductors.

And the inductance begins to drop with the increase of the current. At full load, the two-permeability inductor has the same inductance with the single-permeability inductor. To evaluate the efficiency performances of the two inductors, both inductors are tested in a 5-V-input, 3.3-V-output buck converter. The switching frequency of the converter is 750 kHz. Low FOM (figure of merit) MOSFETs are selected as switching devices. Their parameters are listed in Table II. The current ripple waveforms of both the inductors at 3-A output current are illustrated in Fig. 25. The peak-to-peak value of single-permeability inductor is 4.64 A, while that of the two-permeability inductor is 3.82 A. The measured efficiencies of the converter with two inductor prototypes are shown in Fig. 26. The converter has higher efficiency when the two-permeability inductor is used.

IV. Conclusion

This paper proposed a two-permeability inductor structure to improve unevenly distributed flux density of planar distributed air-gap inductors; comparison and analysis of such inductors with single-permeability inductors are demonstrated with the aid of FEA simulation. Based on the two-permeability structure, inductance could be increased for the improvement of the internal flux density distribution. And for the same reason, the two-permeability inductor has higher core loss and ac winding loss. Two prototypes of the same volume are fabricated based on the LTCC technology; one is single permeability, and the other one is two-permeability. The experimental results show that the two-permeability inductor has higher inductance than the single permeability one, and could improve maximum 0.5% efficiency of a dc/dc converter.

References

[1] G. Chinn, S. Desai, E. DiStefano, K. Ravichandran, and S. Thakkar, "Mobile PC platforms enabled with INTEL CENTRINO mobile technology," *Intel Technol. J.*, vol. 7, no. 2, pp. 6–15, May 2003.

[2] L. Qiang, M. Lim, J. Sun, A. Ball, Y. Ying, F. C. Lee, and K. D. T. Ngo, "Technology road map for high frequency integrated DC-DC converter," in *Proc. IEEE Appl. Power Electron. Conf.*, 2010, pp. 533–539.

[3] S. Iyengar, T. M. Liakopoulos, and C. H. Ahn, "A DC/DC boost converter toward fully on-chip integration using new micromachined planar inductors," in *Proc. Power Electron. Spec. Conf.*, 1999, pp. 72–76.

[4] Y. Katayama, S. Sugahara, H. Nakazawa, and M. Edo, "High-Power-Density MHz-Switcing Monolithic DC-DC Converter with Thin-Film Inductor," in *Proc. Power Electron. Spec. Conf.*, 2000, pp. 1485–1490.

[5] P. Dhagat, S. Prabhakaran, and C. R. Sullivan, "Comparison of magnetic materials for V-groove inductors in optimized high-frequency DC-DC converters," *IEEE Trans. Magn.*, vol. 40, no. 4, pp. 2008–2010, Jul. 2004.

[6] C. R. Sullivan and S. R. Sanders, "Design of microfabricated transformers and inductors for high-frequency power conversion," *IEEE Trans. Power Electron.*, vol. 11, no. 2, pp. 228–238, Mar. 1996.

[7] M. H. Lim, J. D. Van Wyk, F. C. Lee, and K. D. T. Ngo, "A class of ceramic-based chip inductors for hybrid integration in power supplies," *IEEE Trans. Power Electron.*, vol. 23, no. 3, pp. 1556–1564, May 2008.

[8] E. Waffenschmidt, B. Ackermann, and J. A. Ferreira, "Design method and material technologies for passives in printed circuit Board Embedded circuits," *IEEE Trans. Power Electron.*, vol. 20, no. 3, pp. 576–584, May 2005.

[9] M. Ludwig, M. Duffy, T. O'Donnell, P. McCloskey, and S. C. Ó Mathùna, "PCB integrated inductors for low power DC/DC converter," *IEEE Trans. Power Electron.*, vol. 18, no. 4, pp. 937–945, Jul. 2003.

[10] J. A. Cobos, M. Rascon, L. Alvarez, S. Ollero, M. De Graf, and W. Waanders, "Low profile and low output voltage DC/DC converters for on-board power distribution using planar magnetics," in *Proc. Ind. Appl. Conf.*, 1997, pp. 1153–1158.

[11] A. H. Feingold, M. Heinz, and R. L. Wahlers, "Compliant dielectric and magnetic materials for buried components," in *Proc. IMAPS*, vol. 4931, 2002, pp. 65–70.

[12] C.-Y. Kim, H.-J. Kim, and J.-R. Kim, "An integrated LTCC inductor embedding NiZn ferrite," *IEEE Trans. Magn.*, vol. 42, no. 10, pp. 2840–2842, Oct. 2006.

[13] A. W. Roesler, J. M. Schare, S. J. Glass, K. G. Ewsuk, G. Slama, D. Abel, and D. Schofield, "Planar LTCC transformers for high-voltage flyback converters," *IEEE Trans. Compon. Packag. Technol.*, vol. 33, no. 2, pp. 359–372, Jun. 2010.

[14] L. Wang, Y. Pei, X. Yang, X. Cui, and Z. Wang, "Design of multi-turn LTCC inductors for high frequency DC/DC converters," in *Proc. IEEE Appl. Power Electron. Conf.*, 2010, pp. 1610–1615.

[15] M. H. Lim, Z. Liang, and J. D. Van Wyk, "Low profile integratable inductor fabricated based on LTCC technology for microprocessor power delivery applications," in *Proc. IEEE Appl. Power Electron. Conf.*, 2006, pp. 593–599.

[16] M. H. Lim, J. D. Van Wyk, and Z. Liang, "Internal geometry variation of LTCC inductors to improve light-load efficiency of DC-DC converters," *IEEE Trans. Compon. Packag. Technol.*, vol. 32, no. 1, pp. 3–11, Mar. 2009.

[17] Y. Su, Q. Li, M. Mu, D. Gilham, D. Reusch, and F. C Lee, "Low profile LTCC inductor substrate for multi-MHz integrated POL converter," in *Proc. IEEE Appl. Power Electron. Conf.*, 2012, pp. 1331–1337.

[18] D. Reusch, D. Gilham, Y. Su, and F. C. Lee, "Gallium Nitride based 3D integrated non-isolated point of load module," in *Proc. IEEE Appl. Power Electron. Conf.*, 2012, pp. 38–45.

[19] L. Wang, Y. Pei, X. Yang, and Z. Wang, "Design of ultrathin LTCC coupled inductors for compact DC/DC converters," *IEEE Trans. Power Electron.*, vol. 26, no. 9, pp. 2528–2541, Sep. 2011.

[20] L. Wang, Y. Pei, X. Yang, Y. Qin, and Z. Wang, "Improving light and intermediate load efficiencies of buck converters with planar nonlinear inductors and variable on time control," *IEEE Trans. Power Electron.*, vol. 27, no. 1, pp. 342–353, Jan. 2012.

[21] L. Wang, Y. Pei, X. Yang, Z. Wang, and Y.-F. Liu, "A horizontal-winding multi-permeability distributed air-gap inductor," in *Proc. IEEE Ind. Appl. Conf.*, 2012, pp. 994–1001.

[22] J. Lee, Y.-K. Hong, S. Bae, J. Jalli, J. Park, G. S. Abo, G. W. Donohoe, and B.-C. Choi, "Integrated ferrite film inductor for power system-on-chip (PowerSoC) smart phone applications," *IEEE Trans. Magn.*, vol. 47, no. 2, pp. 304–307, Feb. 2011.

[23] Q. Li, Y. Dong, F. C. Lee, and D. Gilham, "High-density low-profile coupled inductor design for integrated point-of-load converters," *IEEE Trans. Power Electron.*, vol. 28, no. 1, pp. 547–554, Jan. 2013.

[24] M. Wang, J. Li, K. D. T. Ngo, and H. Xie, "A surface-mountable microfabricated power inductor in silicon for ultracompact power supplies," *IEEE Trans. Power Electron.*, vol. 26, no. 5, pp. 1310–1315, May 2011.

[25] J. Qiu and C. R. Sullivan, "Inductor design for VHF tapped-inductor dc-dc power converters," in *Proc. IEEE Ind. Appl. Conf.*, Mar. 6–11, 2011, pp. 142–149.

[26] C. O. Mathúna, N. Wang, S. Kulkarni, and S. Roy, "Review of integrated magnetics for power supply on chip (PwrSoC)," *IEEE Trans. Power Electron.*, vol. 27, no. 11, pp. 4799–4816, Nov. 2012.

[27] (2013). [Online]. Available: http://www.coilcraft.com/xpl2010.cfm
[28] (2013). [Online]. Available: http://www.epcos.com/web/generator/Web/Sections/ProductCatalog/Inductors/Page,locale=en.html
[29] (2013). [Online]. Available: http://www.epcos.com/inf/80/ap/e0001000.htm
[30] (2013). [Online]. Available: http://www.electroscience.com/ceramictapes.html
[31] (2013). [Online]. Available: http://www.electroscience.com/ceramictapes.html
[32] C. P. Steinmetz, "On the law of hysteresis," *Proc. IEEE*, vol. 72, pp. 196–221, Feb. 1984.
[33] Q. Li, M. Mu, and F. C. Lee, "Analytical core loss models for planar inductors with non-uniform flux distribution and non-sinusoidal excitation," in *Proc. IEEE Appl. Power Electron. Conf.*, Feb. 5–9, 2012, pp. 1783–1789.

Laili Wang (S'07–M'13) was born in Shaanxi province, China, in 1982. He received the B.S., M.S., and Ph.D. degrees in electrical engineering from Xi'an Jiaotong University, Xi'an, China, in 2004, 2007, and 2011, respectively.

Since 2011, he has been a Postdoctoral Research Fellow in the Department of Electrical Engineering, Queen's University, Kingston, ON, Canada. His research focuses on package and integration of passive devices in high-frequency high-power density dc/dc converters.

Zhiyuan Hu (S'10) received the M.Sc. degree from the University of Ottawa, Ottawa, ON, Canada, in 2010. He is currently working toward the Ph.D. degree in electrical engineering at Queen's University, Kingston, ON.

From 2007 to 2010, he was with Potentia Semiconductor Corp. and Power Integrations Inc. in the area of reference design and IC validation for power management ICs. His research interests include resonant converters, digital control, digital communication for isolated power supplies, and power factor correction. He has one U.S. patent pending.

Dr. Hu received conference travel awards from IAS-PELS and PSMA as a student.

Yan-Fei Liu (M'94–SM'97–F'13) received the Ph.D. degree from the Department of Electrical and Computer Engineering, Queen's University, Kingston, ON, Canada, in 1994.

From February 1994 to July 1999, he was a Technical Advisor with the Advanced Power System Division of Nortel Networks. Since 1999, he has been with Queen's University, Kingston, ON. He is currently a Professor in the Department of Electrical and Computer Engineering. His research interests include digital control technologies for high efficiency, fast dynamic response dc–dc switching converter and ac–dc converter with power factor correction, resonant converters and server power supplies, and LED drivers. He holds 22 U.S. patents and has published more than 130 technical papers in IEEE Transactions and conferences. He is also a principal contributor for two IEEE standards.

Dr. Liu serves as an Associate Editor for the IEEE TRANSACTIONS ON POWER ELECTRONICS since 2001, an Editor-in-Chief for special issue of Power Supply on Chip of the IEEE TRANSACTIONS ON POWER ELECTRONICS, as well as technical program Cochair for ECCE, 2011. He also serves as a Chair for the IEEE Power Electrical Society Technical Committee on Power Conversion Systems and Components.

Yunqing Pei (M'05) was born in 1969. He received the B.S. and M.S. degrees from Xi'an Jiaotong University, Xi'an, China, in 1991 and 1994, respectively, both in electrical engineering, and in 1999, received the Ph.D. degree in power electronics.

He was a Faulty Member of Xi'an Jiaotong University, where he is currently an Associate Professor. From February 2006 to February 2007, he was a visiting scholar of the Center of Power Electronics Systems, Virginia Polytechnic Institute and State University, Blacksburg, VA, USA. His research interests include high-power inverters, switch mode power supply, and converters in distributed generation systems.

Xu Yang (M'02) was born in China, in 1972. He received the B.S. and Ph.D. degrees in electrical engineering from Xi'an Jiaotong University, Xi'an, China, in 1994 and 1999, respectively.

He has been a Faculty Member of the faculty of School of Electrical Engineering, Xi'an Jiaotong University, since 1999, where he is currently a Professor. From November 2004 to November 2005, he was with the Center of Power Electronics Systems, Virginia Polytechnic Institute and State University, Blacksburg, VA, as a Visiting Scholar. He then came back to Xi'an Jiaotong University, and was involved in the teaching and research in power electronics and industrial automation area. His research interests include soft switching topologies, PWM control techniques and power electronic integration, and packaging technologies.

Zhaoan Wang (SM'98) was born in China, in 1945. He received the B.S. and M.S. degrees in electrical engineering from Xi'an Jiaotong University, Xi'an, China, in 1970 and 1982, respectively, and the Ph.D. degree in electrical engineering from Osaka University, Osaka, Japan, in 1989.

From 1970 to 1979, he was a Researcher in the Xi'an Power Rectifier Factory and became a Teacher in Xi'an Jiaotong University, in 1982. In 1989, he came back to Xi'an Jiaotong University from Japan and has been involved in teaching and researching in the areas of power electronics and industrial automation. His research interests include power conversion systems, harmonics suppression and reactive power compensation, active power filters, power electronic integration, and packaging technologies.